J Mol Model (2011) 17:2501–2511
DOI 10.1007/s00894-010-0933-z

ORIGINAL PAPER

Topological description of the bond-breaking and bond-forming processes of the alkene protonation reaction in zeolite chemistry: an AIM study

María Fernanda Zalazar · Nélida Maria Peruchena

Received: 2 September 2010 / Accepted: 8 December 2010 / Published online: 31 December 2010

Abstract Density functional theory and atoms in molecules theory were used to study bond breakage and bond formation in the trans-2-butene protonation reaction in an acidic zeolitic cluster. The progress of this reaction along the intrinsic reaction coordinate, in terms of several topological properties of relevant bond critical points and atomic properties of the key atoms involved in these concerted mechanisms, were analyzed in depth. At B3LYP/6-31++G(d,p)//B3LYP/6-31G(d,p) level, the results explained the electron density redistributions associated with the progressive bond breakage and bond formation of the reaction under study, as well as the profiles of the electronic flow between the different atomic basins involved in these electron reorganization processes. In addition, we found a useful set of topological indicators that are useful to show what is happening in each bond/atom involved in the reaction site as the reaction progresses.

Keywords Acid-catalyzed alkenes protonation · Electron density · Carbenium ion · Heterogeneous catalysis · Intrinsic reaction coordinate · Catalysis

Electronic supplementary material The online version of this article (doi:10.1007/s00894-010-0933-z) contains supplementary material, which is available to authorized users.

M. F. Zalazar · N. M. Peruchena (✉)
Laboratorio de Estructura Molecular y Propiedades,
Área de Química Física, Departamento de Química,
Facultad de Ciencias Exactas y Naturales y Agrimensura,
Universidad Nacional del Nordeste,
Avenida Libertad 5460,
3400 Corrientes, Argentina
e-mail: arabeshai@yahoo.com.ar

M. F. Zalazar
Facultad Regional Resistencia,
Universidad Tecnológica Nacional,
French 414,
3500 Resistencia, Chaco, Argentina

Introduction

Zeolites are microporous aluminosilicate minerals that are used widely in the chemical industry. Due to their high selectivity, their reactivity and the presence of Brønsted acid sites, acidic zeolites act as solid acid/base catalysts in a variety of reactions [1–4]. Principally, the alkene protonation reactions by acid zeolites feature prominently in many zeolite-catalyzed hydrocarbon transformations of great industrial importance [1, 5] such as dimerization and oligomerization of olefins, and double bond isomerizations.

Prior to the protonation reaction, the interaction of the alkene molecule with the zeolite Brønsted acid site results in the formation of an adsorbed alkene or π complex (Eq. 1). The adsorbed alkene then acts as a reactant in the protonation reaction (Eq. 2), as shown in Scheme 1.

$$\mathrm{T5{-}OH} + \mathrm{C_4H_8} \rightarrow [\mathrm{T5{-}OH\cdots C_4H_8}]_{\mathrm{ads}} \quad (1)$$

$$[\mathrm{T5{-}OH\cdots C_4H_8}]_{\mathrm{ads}} \rightarrow [\mathrm{T5{-}O^{-}C_4H_9^{+}}]^{\neq} \rightarrow \mathrm{T5{-}O{-}C_4H_9} \quad (2)$$

Since the pioneering work of Kazansky [15], the mechanism of the initial protonation of light alkenes over the Brønsted acid sites of zeolites has been studied extensively using diverse experimental methods [6–8] and theoretical calculations [9–14]. Within the broad scope of these theoretical investigations, particular interest has

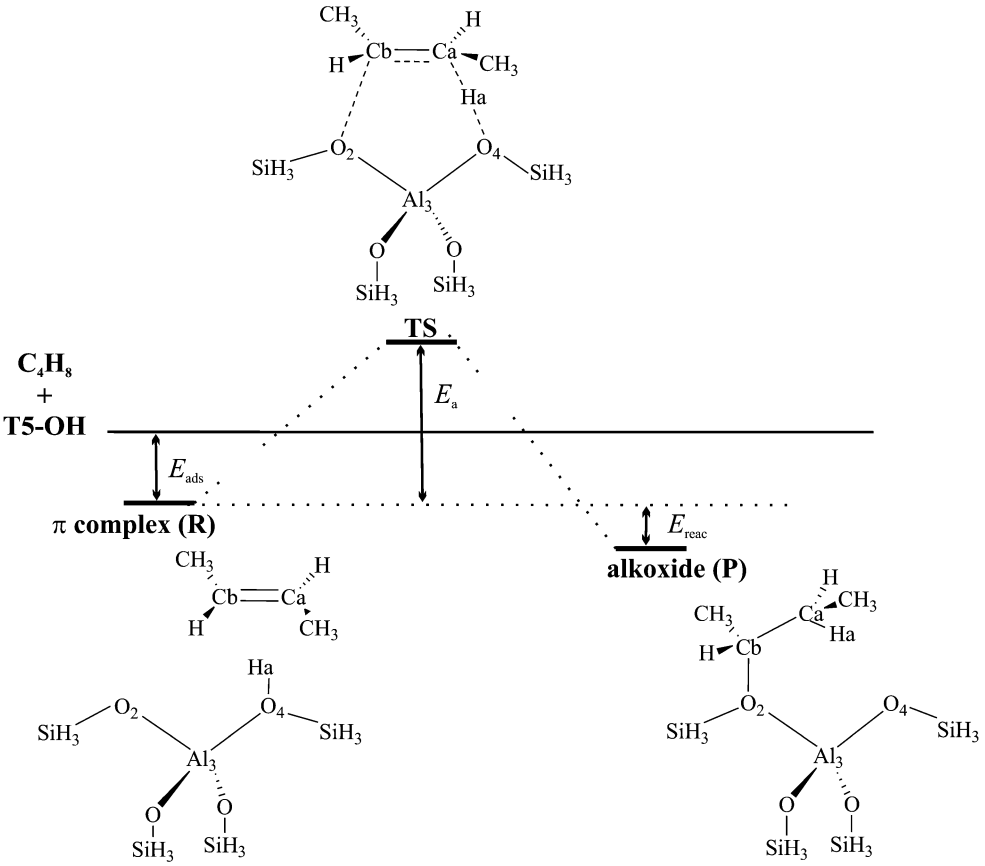

Scheme 1 Structures of adsorbed alkene on a Brønsted acid site (R), transition state (TS) for olefin protonation reaction, and alkoxide product (P)

focused on extracting information about the stationary points of the potential energy surface. Carbocations and alkoxides are accepted as reaction intermediates in acid-catalyzed hydrocarbon reactions; however, the mode of formation as well as the true nature of these intermediaries is still a matter of controversy [16]. The protonation of an olefin by an acid hydroxyl group results in the formation of a more stable alkoxide product (P), in which the process is concerted and occurs through a transition state (TS), wherein the organic fragment resembles that of a classical carbenium ion. In the course of the reaction, the hydrogen atom of the Brønsted acid site, H_a, protonates a carbon atom of the olefin double bond, C_a. Simultaneously, the positive charge that appears on C_b interacts with one of the neighboring basic oxygen atoms of the zeolite, O_2, giving rise to the formation of a C_b–O_2 bond, and, consequently, the formation of the alkoxide product.

In order to provide a better understanding of the details of the electron redistribution upon chemical transformations, we investigated in a previous work [17] the electron density properties of the stationary points of the ethene protonation reaction by an acidic zeolite, in the framework of the quantum theory of atoms in molecules (QTAIM) [18, 19]. This approach allows clear insight into the nature and properties of the chemical bonds between the interacting species. Although this methodology has been applied successfully to a variety of chemical systems [20], only a very few theoretical studies have reported any topological analysis of the electron density, $\rho(r)$, in zeolite chemistry [17, 21–27]. As we found previously [17], the most important topological feature in this process is the electron charge density redistribution. The alkoxide product is formed as a consequence of the electrophilic strength developed by the positively charged C_b atom; this atom withdraws electrons from the atomic basin of the (basic) O_2 atom, which acts as a Lewis basic site. As the reactions proceed, an electronic redistribution in both the alkene fragment and the zeolite cluster is produced.

In an attempt to extend our knowledge of the course of these chemical reactions, we considered it interesting to study electron density redistribution, not only on the stationary points, but also associated with the topological changes along the intrinsic reaction coordinate (IRC). Analysis of the electron density along the IRC path has been used by several co-workers and has proved useful in analyzing reactions similar to those described here. The keto–enol tautomerism of an acetaldehyde, the pinacol rearrangement of a protonated 1,2-ethanediol, and the unimolecular decomposition of the methanediol, were studied as examples of hydrogen transfer [28]. Additionally, two possible reaction pathways were studied in the Lewis acid mediated reaction of acetonitrile and benzonitrile oxide

[29]. Furthermore, the atoms in molecules (AIM) theory was applied to non-stationary states along the IRC in a topological analysis of S_N2 reactions of methyl halides [30]. Also, the properties of bond critical points (BCP) along the IRC were used to establish a quantitative structure–property relationship in calculated reaction pathways [31]. Thus, QTAIM analysis can be used in the discussion of the electron redistribution experienced in such reactions.

In a similar sense, in this work we carried out an analysis of the trans-2-butene reaction protonation by an acidic zeolitic cluster within the framework of the AIM theory by evaluating changes in bond and atomic properties along the IRC. Although several theoretical studies have been performed on these reactions, to our knowledge none have included an electron density topological analysis or computation of atomic properties to describe the evolution of changes along the IRC. Therefore, we analyzed bond breakage and bond formation during this process in order to give topological indicators that show what is happening in each bond/atom involved in the reaction site. To this end, we used topological characterization at BCP in several bonds along the reaction path, as well as a description of the evolution of some of the atomic properties during this concerted process in order to understand the electronic transference between the alkenes and the catalyst as well as the stabilization/destabilization undergone by atoms involved in the reaction site. Furthermore, we demonstrate that analysis of electron density distribution profiles along the IRC is a powerful tool that allows us to visualize the flow of electrons between the different atomic basins involved in the reaction.

Methods and calculation details

We selected trans-2-butene as a candidate for the description of the chemical reaction of the alkenes protonation reaction catalyzed by acidic zeolites along the IRC. This alkene molecule is useful when considering the secondary nature of olefinic carbons. The zeolite catalyst was modeled by a widely used cluster, $H_3Si–OH–Al(–O–SiH_3)_3$, denoted T5–OH, because this model provides a good description of the bifunctional nature of zeolite active sites and includes, as far as possible, both short- and medium-range electrostatic effects [11, 17].

The geometries of all species were optimized without any constraints. Hybrid density functional theory (DFT) calculations at the Becke3 Lee–Yang–Parr (B3LYP) level [32, 33] with the 6-31G** basis set were carried out using the Gaussian 03 suite of programs [34]. All stationary points were characterized by calculating the Hessian matrix and analyzing vibrational normal modes. Starting at the TS, we calculated the reaction pathways in forward and reverse directions in order to investigate the minima connected by the TS. The reaction path was followed employing the IRC algorithm [35, 36], as implemented in Gaussian 03. A step size of 0.01 $amu^{1/2}$Bohr was used.

A topological analysis of the electron charge density distribution, $\rho(r)$, in the framework of AIM theory [18–20] was carried out for the present study. Total electron densities were obtained at B3LYP level with the 6-31++G** basis set. The bond and atomic properties were calculated using the Aim2000 package [37]. Certain structures on the reaction pathway were selected for the electron density analysis. The reaction process was investigated using the AIM partition scheme of electron charge density. In this work, we calculated variations in typical electron density properties calculated at the BCP in order to characterize bond breakage and bond formation. Moreover, we calculated the variations in the integrated atomic properties over the atomic basin along the corresponding IRC path.

Overview of AIM theory

Here, we present only the essential theoretical information needed for discussion of the results, because the use of topological concepts is well documented in the standard literature [18–20]. The electron charge density, $\rho(r)$, is a physical quantity that has a definite value at each point in space. According to AIM theory, an atom in a molecule is defined as the union of an attractor and its associated basin, called an atomic basin. It is bounded by a zero-flux surface in the gradient vector field of the charge density, $\nabla\rho(r)$, which defines an atomic boundary. When two atoms share some portion of their surfaces, a line of maximum electronic charge density is formed between the nuclei, and, at the point where the shared surface intersects this atomic interaction line or bond path, there is a saddle point in $\rho(r)$ called a bond critical point (BCP). In this manner, the AIM theory identifies a unique line of communication between two chemically interacting nuclei, and provides a unique point where it is possible to probe or characterize this interaction.

In AIM theory, an interaction is characterized by: (1) the charge density at the critical point, ρ_b, as a measure of how much charge is accumulated between the bonded nuclei and reflects the strength of a bond; (2) the Laplacian $\nabla^2\rho_b$ as a measure of local charge concentration ($\nabla^2\rho_b < 0$) or local charge depletion ($\nabla^2\rho_b > 0$); (3) the ellipticity, ε, as a measure of the π character of a bond but also of its structural stability. Finally, from a topological point of view, the covalent character of an interaction is analyzed quantitatively by taking into account the $|V_b|/G_b$ relationship, where V_b and G_b are the potential and the kinetic energy densities evaluated at the BCP.

Results and discussion

The electron density properties of the stationary points of the ethene protonation reaction catalyzed by acidic zeolite have been investigated recently [17]. Analysis of the global process shows that the bonds that change their properties more significantly are H_a–O_4, C_a···H_a, C_a–C_b and C_b···O_2. Consequently, in the present work, the electron density properties of the aforementioned bonds, for the trans-2-butene protonation reaction on the surface extrema (reactant and product), and their variation along the IRC, will be described separately in the following paragraphs.

Bond distances and local topological properties [electron densities (ρ_b), the Laplacian ($\nabla^2\rho_b$), the relationship between the local potential energy density and the local kinetic energy density ($|V_b|/G_b$), and the ellipticity (ε)] of the surface extrema are listed in Table 1. The results in Table 1 are in accordance with previously published data on the ethene protonation reaction and therefore will not be discussed in detail.

Table 1 shows that the topological properties at the BCP on the C_a–C_b and O_4–H_a bonds in the π complex, **R**, are clearly indicative of shared interactions. Also, the C_a···H_a interaction shows characteristics of a closed shell interaction. In the alkoxide, **P**, the absence of a BCP between the O_4 and H_a atoms indicates that the O_4–H_a bond was broken, whereas a new bond was formed between the O_2 and C_b atoms (the C_b···O_2 interaction is absent in R). The topological properties at the BCP of the C_b···O_2 bond (formed in **P**) show that this bond can be defined as a weak shared interaction.

The electronic changes along the reaction coordinate reflect the thermochemistry of the trans-2-butene protonation reaction. Our calculation predicts an activation energy of 26.02 kcal mol^{-1} (see Scheme 1). The formation of **P** was observed to be exothermic, and the calculated reaction energy (**P** energy relative to the physisorbed π complex energy) was −6.61kcal mol^{-1}. These results are in accordance with results obtained by other authors [12]. Moreover, the global energy variation and the geometrical distance of the selected bonds along the IRC for trans-2-butene protonation reaction by acidic zeolite are shown in Figs. S1 and S2 in the Electronic Supplementary Material.

Evolution of the local properties of $\rho_{(r)}$ during the protonation reaction

Local topological properties of electron density calculated at the BCP along the IRC provide interesting information on bond breakage and bond formation for the reaction under study and allowed us to characterize the interactions between the atoms involved in the reaction site. Figure 1 shows the variation in local topological properties at the BCPs along the IRC corresponding to the interactions involved at the reaction site for the trans-2-butene protonation reaction catalyzed by acidic zeolite. The extreme values for the π complex and the alkoxide product were introduced in Table 1.

As can be seen in Fig. 1a–c, the changes seen in ρ_b, $\nabla^2\rho_b$ and $|V_b|/G_b$ at the selected BCP along the IRC are very pronounced. The electron charge density at C_a···H_a and C_b···O_2 BCPs increases as a result of the formation of these bonds, with a subsequent increase in their strengths. Both the C_a···H_a and C_b···O_2 bonds are stabilized by the increased accumulation of charge density between them. This viewpoint will be discussed in detail below. In addition, Fig. 1a–c shows that the greatest rate of change in local topological properties at BCPs, corresponding to the H_a···O_4 and C_a···H_a bonds, is located in the region between −1.5 and +1.2 $amu^{1/2}$Bohr of the reaction coordinate. In this region, the H_a···O_4 distances lie between 1.03 and 1.66 Å, and the C_a···H_a distances lie in the 1.68–1.14 Å range. In addition, it is interesting to highlight that the proton is linked by bond paths to the O_4 atom and simultaneously to the C_a atom. This implies that the H_a proton is shared between the two atoms, and that it becomes dicoordinated, i.e., C_a···H_a···O_4.

Table 1 Bond distances (Å) and local topological properties (au) of the electron charge density distribution calculated at the position of the bond critical points (BCP) of selected bond paths for reactant (R) and product (P). ρ_b Electron densities, $\nabla^2\rho_b$ the Laplacian, $|V_b|/G_b$ the relationship between the local potential energy density and the local kinetic energy density, ε ellipticity

Bond X-Y	Species	$d_{X\text{-}Y}$	ρ_b	$\nabla^2\rho_b$	ε	$\lvert V_b\rvert/G_b$
H_a–O_4	R	0.988	0.3286	–1.8822	0.0126	8.6917
	P	4.884	–	–	–	–
C_a···H_a	R	2.161	0.0233	0.0465	0.8420	0.9761
	P	1.097	0.2772	–0.9417	0.0095	7.1135
C_a–C_b	R	1.344	0.3409	–0.9727	0.3686	3.8300
	P	1.527	0.2531	–0.6016	0.0314	4.6294
C_b···O_2	R	3.946	–	–	–	–
	P	1.493	0.2058	–0.2839	0.0294	2.4001

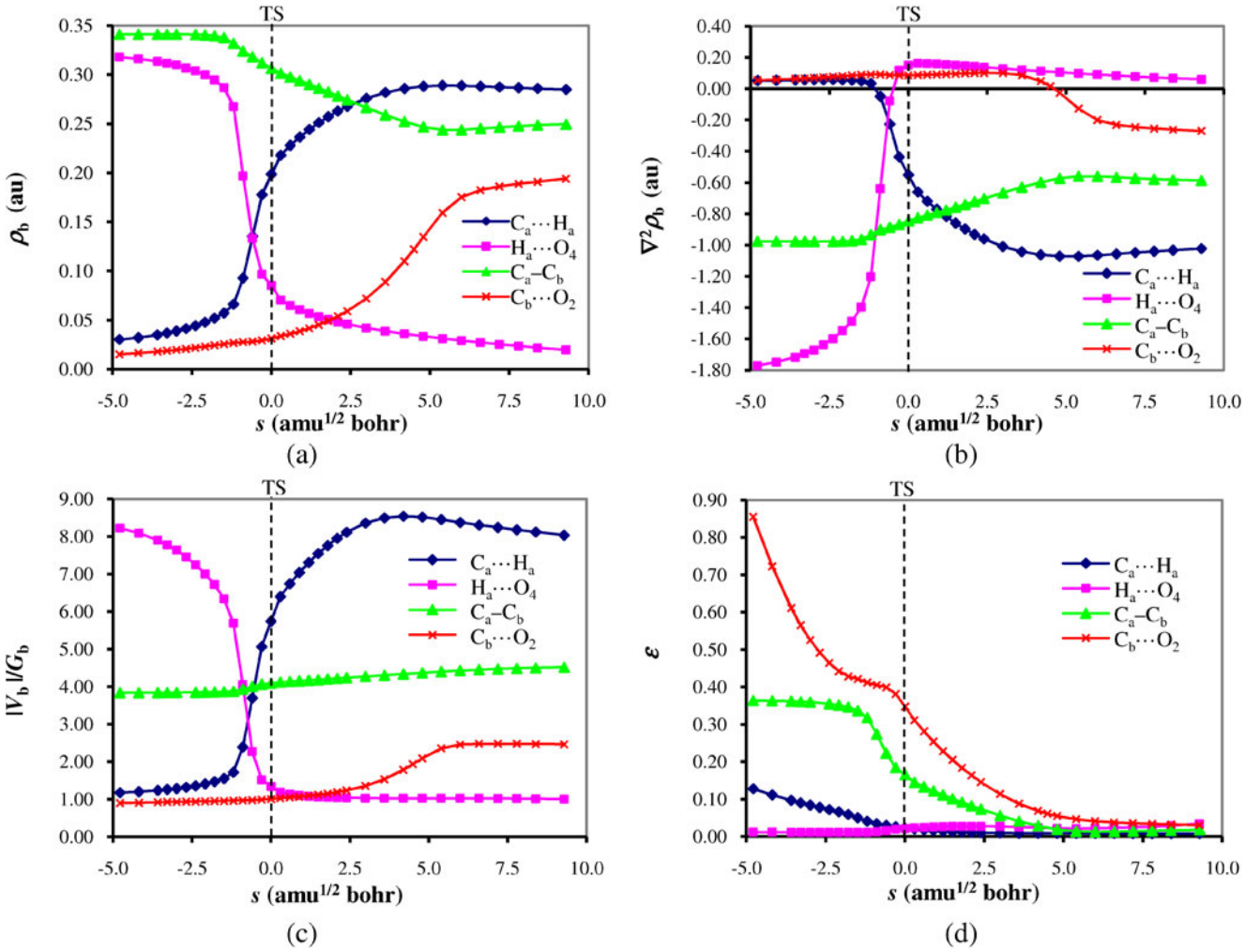

Fig. 1 Variations in local topological properties at selected bond critical points (BCP) along the intrinsic reaction coordinate (IRC) for the trans-2-butene protonation reaction catalyzed by acidic zeolite. **a** Electron density, **b** Laplacian, **c** relationship between local potential energy density and local kinetic energy density, **d** ellipticity. The transition state (TS) is located at the value s = 0.0 of the reaction coordinate

$H_a\cdots O_4$ BCP

Figure 1a shows a strong decrease in electron density at $H_a\cdots O_4$ BCP, which indicates that the $H_a\cdots O_4$ bond weakens to its final breakage (the lower the ρ_b value at the BCP, the lower the strength of the bond). In Fig. 1b, it can be observed that the $\nabla^2\rho_b$ value increases sharply and changes sign near the TS, corresponding to a bond distance of 1.43 Å. This is indicative of the change in nature of this bond. The $H_a\cdots O_4$ bond loses the characteristics of a shared interaction ($\nabla^2\rho_b < 0$) to become a closed shell interaction ($\nabla^2\rho_b > 0$) with some contribution of covalent character in the TS, whereas in the product this interaction is not present, namely, a H_a–O_4 BCP is not found in the alkoxide product, reflecting the rupture of the bond between the H_a and O_4 atoms. The $|V_b|/G_b$ relationship along the IRC shows a strong decrease approaching the TS, becoming less as it reaches a $|V_b|/G_b$ value near to 1 au. This is indicative of a reduction of the covalent character in the first place, with subsequent weakening of the interaction, finally leading to bond breaking process as a consequence. The ellipticity, on the other hand, shows no significant change.

$C_a\cdots H_a$ BCP

Meanwhile, the opposite behavior is observed for the $C_a\cdots H_a$ bond that is being formed at the same time. The electron density at the $C_a\cdots H_a$ BCP increases strongly along the IRC to reach an approximately constant value characteristic of a covalent bond (0.27 au). Regarding the Laplacian, Fig. 1b shows a sign change in the $\nabla^2\rho_b$ values at the reaction coordinate, s, equal to −0.9 amu$^{1/2}$Bohr, equivalent to a $C_a\cdots H_a$ distance of 1.51 Å, and, as a

consequence, a C_a–H_a bond is formed. Moreover, the variation in the $\nabla^2\rho_b$ value confirms these trends with an increasing negative value, reflecting a local concentration of electronic charge in the internuclear $C_a\cdots H_a$ region. As can be observed in Fig. 1c, the $|V_b|/G_b$ relationship at $C_a\cdots H_a$ BCP is > 1 and increases when going from the π complex to the TS. In the first part of the IRC, the $|V_b|/G_b$ relationship is approximately constant and has a value of less than 2. Consequently, the $C_a\cdots H_a$ interaction shows topological characteristics of closed shell interactions. Then, in the vicinity of the TS, an abrupt increase in $|V_b|/G_b$ values is observed. At the TS, the $C_a\cdots H_a$ interaction shows topological characteristics of a shared interaction ($|V_b|/G_b > 2$), and increases the covalent character along the IRC up to a maximum value of about 8.54 au (at s = +4.2 amu$^{1/2}$Bohr). The $|V_b|/G_b$ relationship then decreases slightly and finally shows a value of 7.11 au in the alkoxide product. These variations in the $|V_b|/G_b$ relationship along the reaction coordinate allow us to explain the progressive formation of the $C_a\cdots H_a$ bond and the subsequent rearrangement or redistribution of electron density in order to stabilize the C_a–H_a bond formed.

C_a–C_b BCP

Analysis of the variation in the local topological properties at the BCP on a C_a–C_b bond shows that ρ_b values remain practically constant up to s = −1.8 amu$^{1/2}$Bohr, and then gradually decrease (up to s = +5.4 amu$^{1/2}$Bohr) together with a gradual increase in $\nabla^2\rho_b$. Both properties change gradually during this part of the reaction (Fig. 1a,b). Finally, a very slight increase in ρ_b values is observed from s = +5.4 amu$^{1/2}$Bohr onwards. The $|V_b|/G_b$ relationship increases slightly and shows no significant change (Fig. 1c). The most significant topological change observed is a strong decrease in ellipticity values as the reaction progresses, reaching very low values at the end of the reaction (Fig. 1d). This decrease reflects the hybridization change process along the IRC of both carbon atoms involved in the C_a–C_b bond. Thus, this bond undergoes a transition from a double to a single bond due to the rupture of the olefin π bond and the lengthening of the C_a–C_b bond. However, the C_a–C_b bond retains its covalent character throughout the course of the reaction. As noted by other authors [38], the ellipticity is sensitive to changes in the anisotropy of the electron density in the bond-forming region. This parameter provides an insightful description of the events occurring along the reaction coordinate, and serves as a sensitive index to monitor the π character of double bonds. In a C–C bond, when ε is large, the bond has a significant π character, and when ε is close to zero, the electron density exhibits the cylindrical character typical of either a single or a triple bond.

$C_b\cdots O_2$ BCP

The $C_b\cdots O_2$ interaction is absent in the reactant. When the C_b atom of the alkene molecule interacts with one of the neighboring basic oxygen atoms of the zeolite (O_2), a new BCP appears. This BCP corresponds to the $C_b\cdots O_2$ bond that is being formed and, consequently, the alkoxide appears. As the reaction proceeds, the ρ_b at the BCP of the $C_b\cdots O_2$ interaction becomes larger, which indicates that the $C_b\cdots O_2$ interaction is becoming stronger. In the first part of the reaction path, a continuous and slight increase in ρ_b values is observed; then, as soon as the ρ_b value exceeds 0.04 au, this increase becomes gradually more pronounced, until it slowly reaches a constant value close to 0.2 au (see Fig. 1a).

Considering that the Laplacian magnifies small changes in the electron density of the bond, it should be interesting to investigate the variation in Laplacian at the $C_b\cdots O_2$ BCP along the IRC (Fig. 1b). In the first part of the reaction path, small fluctuations in $\nabla^2\rho_b$ values can be observed; however, it should be considered that $\nabla^2\rho_b$ remains practically constant during this part of the reaction (maximum variations do not reach 0.05 au). The $\nabla^2\rho_b > 0$ indicates a weak electrostatic interaction between the basic oxygen atom and the electron-deficient carbon (a closed shell interaction). In the second part of the reaction path, a continuous decrease in $\nabla^2\rho_b$ values is observed, and, at approximately s = +4.8 amu$^{1/2}$Bohr (equivalent to a $C_b\cdots O_2$ bond distance of 1.678 Å), the $\nabla^2\rho_b$ value changes its sign. This result is indicative of the change in the character of the interaction, from closed shell to shared interaction, due to the formation of the C_b–O_2 bond. Finally, $\nabla^2\rho_b$ values decrease slowly and reach a value close to the equilibrium value of about −0.2 au (from s = +6.0 amu$^{1/2}$bohr).

In addition, an in depth analysis of the $|V_b|/G_b$ relationship at $C_b\cdots O_2$ BCP along the IRC was performed. Figure 1c shows that the $|V_b|/G_b$ values at the $C_b\cdots O_2$ BCP are positive and increase from reactant to product. However, $|V_b|/G_b$ is < 1 before the TS is reached; this implies that a pure closed shell interaction takes place in this part of the reaction path. Thereafter, up to s = +4.8 amu$^{1/2}$Bohr of the reaction path, the $|V_b|/G_b$ relationship is within the range of 1–2 au; thus, in this part of the reaction path this bond involves an intermediate character between shared interaction and closed shell interaction (the slight gain of potential vs kinetic energy density at the BCP and $\nabla^2\rho > 0$ is indicative of a small degree of covalence in this new bond [39]). Subsequently, the $|V_b|/G_b$ relationship increases in value, reaching a maximum of ~2.4 au in the alkoxide product; $|V_b|/G_b$ values > 2 indicate "weak covalent bond" features for the carbon–oxygen bond as was previously established by our group [17].

Regarding the ellipticity changes, at the beginning of the reaction, it is noticeable that the ellipticity at C–O BCP is of a moderate value (0.85) and then decreases quickly, reaching a value of 0.05, then remains approximately constant until the end of the process (Fig. 1d). These results indicate that, in accordance with what was expressed before, the σ-character of the forming C–O bond is established at a late stage of the reaction (after s = +4.8 amu$^{1/2}$Bohr of the reaction path, when C_b is located at 1.678 Å from the O_2).

In the AIM theory, all information about a particular AIM atom is contained in its finite volume, and its properties can be obtained by integrating each corresponding density property over the atomic basin [18, 19]. The ability to determine individual atomic contributions to changes in charge and energy at a given fragment should be of particular use to obtain a better understanding of the subjacent modification produced along the reaction coordinate. Thus, the next section deals with the atomic properties of atoms involved in the reaction site, with the aim of giving a detailed description of the chemical reaction in terms of the electron density rearrangement process along the IRC.

Evolution of atomic properties during the protonation reaction

A previous study by our group showed that the atoms whose properties are significantly affected by the protonation reaction are the proton that is transferred, both carbon atoms involved in the double bond, and the oxygen atoms at the Brønsted and Lewis site [17]. Consequently, the atomic properties of these atoms at the surface extrema, and their variation along the IRC, will be described separately in the following paragraphs. Table 2 lists the topological atomic properties [atomic net charge, $q_{(\Omega)}$, and atomic energy, $E_{(\Omega)}$] of selected atoms involved in the reaction site of the reactant (R) and the alkoxide product (P). The accuracy of the integration was assessed by the magnitude of a function L (Ω), which, in all cases, is less than 10^{-5} au for H atom and 10^{-4} au for other atoms.

The proton from the acidic hydroxyl group, H_a, increases its electronic population from R to P and, consequently, results stabilized. The oxygen atoms in the acidic and the basic site, O_4 and O_2, respectively, increase/decrease their atomic charge and both become destabilized from reactant to product. On the other hand, both carbon atoms increase their atomic charge and are destabilized from reactant to product. Analysis of the atomic properties of the reactant and product (as well as the TS) provides valuable information about the reaction; however, the electron density redistribution that accompanies bond breaking and bond formation is dominated by the electron exchange between the different basins in the reaction site. As a consequence, and due to the concerted nature of this reaction, it is interesting to investigate this electron exchange in the above-mentioned atoms along the IRC. A profound study of the variation in the AIM atomic charge along the IRC was performed in order to highlight the effect of the charge transfer process between the alkene molecule and the zeolite. The evolution of AIM charges for H_a, C_a and C_b carbons atoms, and O_4 and O_2 oxygen atoms is shown in Fig. 2a–c, respectively. These atoms display the greatest charge transfer during the reaction.

Table 2 Topological atomic properties (in au) of selected atoms in π complex (R) and alkoxide product (P)[a]. $q_{(\Omega)}$ Net atomic charge, $E_{(\Omega)}$ total atomic energy

Atom	Species	$q_{(\Omega)}$	$E_{(\Omega)}$
H_a	R	+0.627	–0.3169
	P	–0.025	–0.6383
O_4	R	–1.514	–75.6276
	P	–1.674	–75.5950
O_2	R	–1.676	–75.5969
	P	–1.416	–75.5869
C_a	R	–0.043	–37.9008
	P	+0.088	–37.8363
C_b	R	–0.044	–37.9021
	P	+0.413	–37.6324

[a] For E, 1 au = 2.625 x10^3 kJ mol^{-1}

Analysis of Fig. 2a–c shows that, of the five atoms involved in the reaction site, the most affected is the acidic hydrogen, H_a. The variations in the AIM atomic properties of the H_a proton that is been transferred are more significant from s = −1.2 amu$^{1/2}$ Bohr onwards. The results show that there is a large decrease in the positive charge of H_a (from 0.62 to 0.04 au). It is important to highlight that the charge on the proton that is been transferred is considered low (0.3 au in the TS). Interestingly, this is due to the H_a being bound to two atoms (C_a and O_4) or the fact that it becomes dicoordinated (i.e.; $C_a \cdots H_a \cdots O_4$). Both atoms mentioned provide electron density to the H_a basin, as was stated in our previous work [17]. On the other hand, the carbon atomic charges vary within a range of 0.36 au in C_b (from +0.02 to +0.38 au) and of 0.21 au in C_a (from −0.12 to +0.09 au). The range of variation for the basic O_2 oxygen atom is only 0.29 au. Finally, the O_4 atom experiences a slight charge variation of about 0.15 au of the global process.

The atomic charge of C_a increases at the end of the reaction, with the increase in net charge being approximately 0.21 au, as expressed previously. However, C_a experiences marked changes throughout the process, achieving a minimum value near the TS (at s around −0.9 amu$^{1/2}$ Bohr). The variations in atomic charge experienced along the

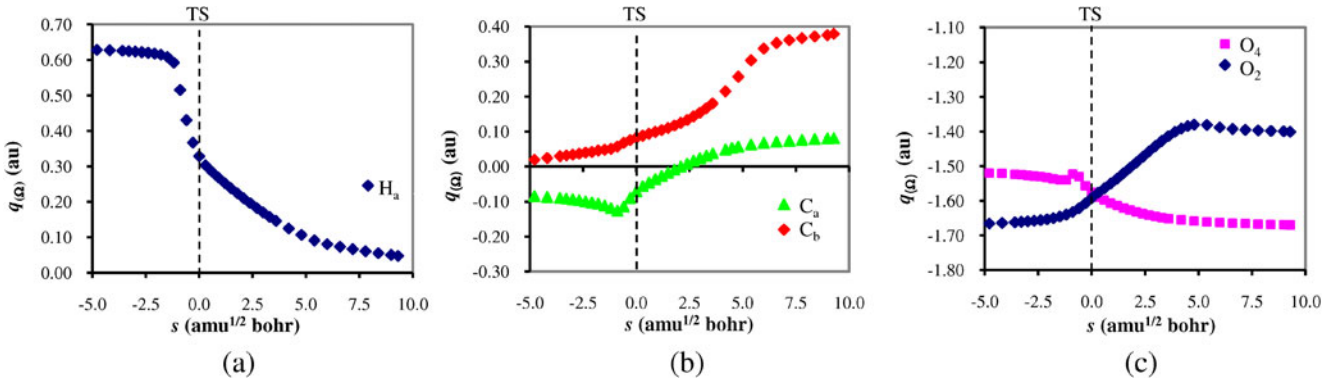

Fig. 2 Atomic net charge profile along the intrinsic reaction paths of the atoms involved in the reaction site. **a** H_a; **b** C_a and C_b; **c** O_2 and O_4. The TS is located at the value s = 0.0 of the reaction coordinate

reaction coordinate indicate that two different stages can be considered for electron charge redistribution of the C_a atom. In the first part of the path, the C_a atom first extracts electrons from the neighboring C_b atom and decreases its atomic charge (via the increase in its electron population). Then, the atomic charge on C_a increases due to the fact that its electron charge density is transferred to the atomic basin of the electrophilic proton that has been transferred from the acid site. At the TS, the atomic charge on C_a is negative, and it changes to positive at s = 2.1 amu$^{1/2}$Bohr (equivalent to a C_a···H_a distance of 1.12 Å). On the other hand, an increase of $q(C_b)$ along the reaction coordinate is observed, reaching an approximately constant value at s = 6.0 amu$^{1/2}$Bohr (this corresponds to the stabilization of the C_b–O_2 bond, as seen already in Fig. 1c). In addition, Fig. 2b shows that both carbon atoms have opposite charges at the TS.

The atomic charges of the oxygen atoms of the acidic and basic site of the zeolite cluster, O_4 and O_2, respectively, display opposite behavior along the IRC path (see Fig. 2c); however, they present similar charges values in the TS. This behavior highlights the bifunctional character of the catalytic site of the protonated zeolite. The loss of electron population in the O_2 atom is higher that the gain of electron population in the O_4 atom. A continuous increase in atomic charge is observed at the O_2 atom along the reaction path (this increase is due to electron donation from O_2 to C_b atom), until it reaches a maximum value at s = 4.8 amu$^{1/2}$Bohr. It then decreases slowly up to the point of stabilization of the O_2 atom. This maximum corresponds to a character change of the forming C_b–O_2 bond (from closed shell to shared interaction, Fig. 1b). The O_4 charge increases due to the fact that the H_a atom transfers its electron density to the former, as it takes electrons from the C_a atom (the migration of H_a from O_4 to C_a is accompanied by a progressive transfer of electron charge from C_a to H_a and from H_a to O_4).

The atomic energies along the reaction coordinate for H_a, C_a and C_b atoms, and O_4 and O_2 atoms are shown in Fig. 3a–c, respectively. It can be observed in Fig. 3a from the $E(H_a)$ values, that this atom is stabilized along the IRC. The trend of the curve is similar to that observed for atomic charge. The stabilization of H_a increases after TS formation. Figure 3b shows that the energy of both carbon atoms decreases before reaching the TS, followed by an increase that results in the destabilization of both atoms. These energies finally reach an approximately constant value that corresponds to the stabilization of the C_b–O_2 shared

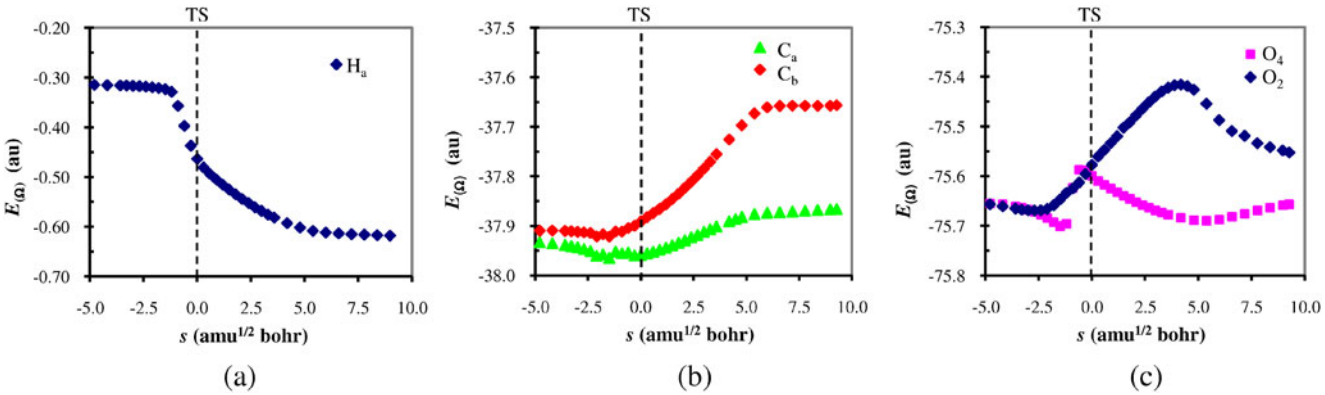

Fig. 3 Atomic energy profile along the intrinsic reaction paths of the atoms involved in the reaction site. **a** H_a; **b** C_a and C_b; **c** O_2 and O_4. The TS is located at the value s = 0.0 of the reaction coordinate

interaction (see Fig. 1b,c). The destabilization of the C_b atom becomes greater than the C_a atom as proton transfer proceeds.

Regarding the oxygen atom energies, the evolution observed for the two oxygen atoms is very different, as can be seen in Fig. 3c. Both curves present a maximum and a minimum at different places in the reaction path. The energy of the O_2 atom decreases up to $s = -2.7$ amu$^{1/2}$Bohr, reaches a maximum at about $s = 4.2$ amu$^{1/2}$Bohr, and then decreases again. This is indicative of a first stabilization, as a consequence of the weak interaction between the oxygen atom of the basic site and the electron deficient carbon atom. The O_2 atom is then destabilized due to electron donation from the O_2 to the C_b atom. The maximum of $E(O_2)$ corresponds to the change in the character of the C_b–O_2 interaction from closed shell to shared interaction, which means that the O_2 atom is stabilized as soon as the C_b–O_2 bond acquires the characteristics of a shared interaction (Fig. 1b).

On the other hand, the atomic energy profile of the O_4 atom shows an unexpected shape. The energy of the O_4 atom decreases up to $s = -1.5$ amu$^{1/2}$Bohr. An abrupt increase is then observed until a maximum energy value is reached (at $s = -0.6$ amu$^{1/2}$bohr); followed by a decrease and a slow final increase of the $E(O_4)$. The first stabilization zone corresponds to the initial slight decrease of ρ_b at $O_4\cdots H_a$ BCP, which means that the O_4 is initially slightly stabilized as the O–H bond lengthens. The zone of abrupt destabilization (between −1.5 to −0.6 amu$^{1/2}$Bohr) corresponds to the rapid decrease of ρ_b at $O_4\cdots H_a$ BCP. The maximum value corresponds to the s coordinate where the Laplacian at the $O_4\cdots H_a$ BCP changes its sign, showing the loss of a shared interaction characteristic (or O_4–H_a bond breaking). After the O_4–H_a bond breaks, the O_4 atom is stabilized and destabilized by the redistribution of electron density.

In summary, we have found that the migration of the H_a atom from O_4 to C_a is accompanied by a progressive transfer of electron charge from C_b to C_a, from C_a to H_a and from H_a to O_4 atoms. Meanwhile, as C_b transfers electrons to C_a, an electronic deficiency in C_b is generated. This electronic deficiency is compensated by getting the electrons from the oxygen atom of the basic site, O_2. Therefore, the charge evolution along the reaction coordinate shows the whole electronic displacement process coming from the atom basins in the site of the reaction in order to achieve stabilization of the product. Bond breakage and bond formation are dominated by the electronic exchange between the different basins in the reaction site.

This electronic displacement along the protonation reaction produces the necessary energetic changes in order to achieve the stabilization of the alkoxide product. Finally, our preliminary results suggest that the electron density redistribution that accompanies the proton transfer (that is, O_4–H_a bond breaking and C_a–H_a bond formation), together with the change from double to single bond at the alkene fragment, determine the activation energy value. These electronic movements, together with the subsequent stabilization of carbocation charge by the zeolitic fragment from the TS toward the alkoxide, determine the global energy of the protonation reaction. However, more data will be required comparing a series of alkenes of greater size. This is currently are under investigation in our laboratory and the results will be published in the near future.

Conclusions

Bond breakage and bond formation during the trans-2-butene protonation reaction catalyzed by acidic zeolites were investigated within the framework of QTAIM, by evaluation of the changes in bonds and atomic properties of the electron density distribution along the IRC. The results revealed that local properties such as ρ_b, $\nabla^2\rho_b$, ε and the $|V_b|/G_b$ relationship, as well as the atomic properties $q_{(\Omega)}$ and $E_{(\Omega)}$, are good indicators to prove what is happening in each bond/atom involved in the reaction site as the reaction progresses.

We found out that the electron density properties at relevant BCPs along the reaction coordinate reveal the progressive formation/breakage of different bonds, and the subsequent redistribution of electron density in order to stabilize the product formed. The variations in the local properties of ρ_b, $\nabla^2\rho_b$ and $|V_b|/G_b$ on H_a–O_4 and C_a–H_a bonds, which are being broken/formed at the same time, show opposite behaviors as the transfer of the proton goes forward, allowing the identification of specific regions during proton transfer. C_a–H_a bond formation and H_a–O_4 bond breakage take place before reaching the TS, in the early part of the reaction, and the process then involves an electronic redistribution. The final H_a–O_4 bond breakage can be inferred by the complete disappearance of the BCP at the end of the reaction. Moreover, three regions involved in the formation of the C_b–O_2 bond were characterized. The first region implies that a pure closed shell interaction takes place between the O_2 and C_b atoms. Consequently, an intermediate character between a shared interaction and a closed shell interaction is observed between them, and finally the carbon–oxygen bond takes on the features of a weak covalent bond. We show that the σ-character of the forming C–O bond is established in the late part of the reaction, in contrast to the C_a–H_a bond that is formed previously.

In addition, although the process is concerted, analysis of the profile of the atomic charges and the atomic energies along the IRC has allowed the electron flow between the different basins involved in the reaction site to be described,

and, at the same time, identified the different regions of this chemical reaction in terms of the charge redistribution process. We discovered that the migration of the H_a atom from O_4 to C_a is accompanied by a progressive transfer of electron charge from C_b to C_a, from C_a to H_a and from H_a to O_4. Meanwhile, as C_b transfers electrons to C_a, an electronic deficiency in C_b is accordingly being generated. This electronic deficiency is compensated by getting the electrons from the oxygen atom of the basic site O_2. Therefore, the charge evolution along the reaction coordinate reveals the whole electronic displacement process coming from the atom basins at the site of the reaction in order to achieve stabilization of the product. Bond breakage and bond formation are dominated by electron exchange between the different basins in the reaction site.

In summary, we characterized not only the net electronic flow, but the mode of formation of the carbocation and its subsequent stabilization to form the alkoxide product. This electronic flow explains how the electronic deficiency on the C_b carbon that will give rise to the carbocation is generated; how its electronic demand is satisfied; and, finally, how it is stabilized as the reaction progresses in order to allow formation of the C_b–O_2 bond that is characteristic of an alkoxide product.

Finally, the present work highlights the potential afforded by electron charge density topological analysis along the IRC (and their atomic properties) for the study of electron redistribution in a selected chemical reaction.

Acknowledgments The authors acknowledge the Secretaria de Ciencia y Tecnología-Universidad Nacional del Nordeste (SECYT-UNNE) for financial support. M.F.Z. is a research fellow of Consejo Nacional de Investigaciones Científicas y Técnicas (CONICET) and N.M.P. is career researcher of Consejo Nacional de Investigaciones Científicas y Técnicas, Argentina. This work was supported by the grant Proyecto de Investigación Científica y Tecnológica Orientado-Universidad Nacional del Nordeste (PICTO-UNNE 089) and Proyecto de Investigación Plurianual-Consejo Nacional de Investigaciones Científicas y Técnicas (PIP-CONICET 00095).

References

1. Corma A (1995) Inorganic solid acids and their use in acid-catalyzed hydrocarbon reactions. Chem Rev 95:559–614. doi:10.1021/cr00035a006
2. Maxwell IE, Stork WHJ (2001) Chapter 17: hydrocarbon processing with zeolites. Stud Surf Sci Catal 137:747–819. doi:10.1016/S0167-2991(01)80259-7
3. Martens JA, Jacobs PA (2001) Chapter 14: introduction to acid catalysis with zeolites in hydrocarbon reactions. Stud Surf Sci Catal 137:633–671. doi:10.1016/S0167-2991(01)80256-1
4. Weitkamp J, Hunger M (2007) Acid and base catalysis on zeolites. Stud Surf Sci Catal 168:787–835. doi:10.1016/S0167-2991(07)80810-X
5. Spoto G, Bordiga S, Ricchiardi G, Scarano D, Zecchina A, Borello E (1994) IR study of ethene and propene oligomerization on H-ZSM-5: hydrogen-bonded precursor formation, initiation and propagation. Mechanisms and structure of the entrapped oligomers. J Chem Soc Faraday Trans 90:2827–2835. doi:10.1039/FT9949002827
6. Datema KP, Nowak AK, van Braam HJ, Wielers AFH (1991) In-situ 13C magic-angle-spinning NMR measurements of the conversion of ethene to aliphatic hydrocarbons over structurally different zeolites. Catal Lett 11:267–276. doi:10.1007/BF00764317
7. Wang W, Jiao J, Jiang Y, Ray SS, Hunger M (2005) Formation and decomposition of surface ethoxy species on acidic zeolite Y. Chem Phys Chem 6:1467–1469. doi:10.1002/cphc.200500262
8. Kazansky VB, Subbotina IR, Jentoft F (2006) Intensities of combination IR bands as an indication of the concerted mechanism of proton transfer from acidic hydroxyl groups in zeolites to the ethylene hydrogen-bonded by protons. J Catal 240:66–72. doi:10.1016/j.jcat.2006.02.028
9. Rozanska X, Demuth T, Hutschka F, Hafner J, van Santen RA (2002) A periodic structure density functional theory study of propylene chemisorption in acidic chabazite: effect of zeolite structure relaxation. J Phys Chem B 106:3248–3254. doi:10.1021/jp011587m
10. Rozanska X, van Santen RA, Demuth T, Hutschka F, Hafner J (2003) A periodic DFT study of isobutene chemisorption in proton-exchanged zeolites: dependence of reactivity on the zeolite framework structure. J Phys Chem B 107:1309–1315. doi:10.1021/jp021646b
11. Boronat M, Zicovich-Wilson CM, Viruela P, Corma A (2001) Influence of the local geometry of zeolite active sites and olefin size on the stability of alkoxide intermediates. J Phys Chem B 105:11169–11177. doi:10.1021/jp011481r
12. Correa RJ, Mota CJA (2002) Theoretical study of protonation of butene isomers on acidic zeolite: the relative stability among primary, secondary and tertiary alkoxy intermediates. Phys Chem Chem Phys 4:375–380. doi:10.1039/b104837f
13. Nieminen V, Sierka M, Murzin DY, Sauer J (2005) Stabilities of C3–C5 alkoxide species inside H-FER zeolite: a hybrid QM/MM study. J Catal 231:393–404. doi:10.1016/j.jcat.2005.01.035
14. Soscún H, Hernández J, Castellano O, Arrieta F, Ruette F, Sierralta A, Machado F, Rosa-Brusin M (2003) The interaction of cis-2-butene over a 10-ring brønsted acid site of zeolite: a theoretical study. J Mol Catal A: Chem 192:63–72. doi:10.1016/S1381-1169(02)00118-8
15. Kazansky VB (1991) The nature of adsorbed carbenium ions as active intermediates in catalysis by solid acids. Acc Chem Res 24:379–383. doi:10.1021/ar00012a004
16. Boronat M, Corma A (2008) Are carbenium and carbonium ions reaction intermediates in zeolite-catalyzed reactions? Appl Catal A: General 336:2–10. doi:10.1016/j.apcata.2007.09.050
17. Zalazar MF, Peruchena NM (2007) Topological analysis of the electronic charge density in the ethene protonation reaction catalyzed by acidic zeolite. J Phys Chem A 111:7848–7859. doi:10.1021/jp071659v
18. Bader RFW (1990) Atoms in molecules. A quantum theory. Clarendon, London
19. Popelier PLA (2000) Atoms in molecules. An introduction. Pearson, Harlow
20. Matta CF, Boyd RJ (2007) The quantum theory of atoms in molecules: from solid state to DNA and drug design. Wiley-VCH, Weinheim
21. Zalazar MF, Duarte DJR, Peruchena NM (2009) Adsorption of alkenes on acidic zeolites. Theoretical study based on the electron charge density. J Phys Chem A 113:13797–13807. doi:10.1021/jp9053814
22. Pidko EA, Hensen EJM, van Santen RA (2008) Anionic oligomerization of ethylene over Ga/ZSM-5 zeolite: a theoretical study. J Phys Chem C 112:19604–19611. doi:10.1021/jp8069767
23. Okulik NB, Pis Diez R, Jubert AH (2003) Topological study of the effect of the isomorphic substitution of silicon by aluminum

on the zeolite structure and its interaction with methane. J Phys Chem A 107:6225–6230. doi:10.1021/jp027399t
24. Okulik NB, Pis Diez R, Jubert AH (2004) A topological study of the transition states of the hydrogen exchange and dehydrogenation reactions of ethane on a zeolite cluster. J Phys Chem A 108:2469–2474. doi:10.1021/jp037149s
25. Okulik NB, Pis Diez R, Jubert AH, Esteves PM, Mota CJA (2001) A topological study of the transition states of the hydrogen exchange and dehydrogenation reactions of methane on a zeolite cluster. J Phys Chem A 105:7079–7084. doi:10.1021/jp0046142
26. Kemner E, de Schepper IM, Kearley GJ (2001) How van der Waals bonds orient molecules in zeolites. Chem Commun: 2466–2467. doi:10.1039/b105611p
27. Soscún H, Castellano O, Hernández J (2004) Adsorption of CH3SH in acidic zeolites: a theoretical study. J Phys Chem B 108:5620–5626. doi:10.1021/jp036468g
28. Mandado M, Mosquera RA, Graña AM, Van Alsenoy C (2005) Charge density analysis of some processes involving intramolecular hydrogen transfer. Tetrahedron 61:819–829. doi:10.1016/j.tet.2004.11.044
29. Wagner G, Danks TN, Vullo V (2007) Quantum-chemical study of the Lewis acid influence on the cycloaddition of benzonitrile oxide to acetonitrile, propyne and propene. Tetrahedron 63:5251–5260. doi:10.1016/j.tet.2007.03.169
30. Ebrahimi A, Roohi H, Habibi M, Karimian T, Vaziri R (2006) Topological and natural population analyses of gas-phase identity SN2 reactions of some methyl halides: backside attack. Chem Phys Lett 419:179–183. doi:10.1016/j.cplett.2005.10.154
31. Alsberg BK, Marchand-Geneste N, King RD (2001) Modeling quantitative structure–property relationships in calculated reaction pathways using a new 3D quantum topological representation. Anal Chim Acta 446:3–13. doi:10.1016/S0003-2670(01)00984-9
32. Becke AD (1993) Density-funtional Thermochemistry. III. The role of exact exchange. J Chem Phys 98:5648–5652. doi:10.1063/1.464913
33. Lee C, Yang W, Parr RG (1988) Development of the Colle-Salvetti correlation-energy formula into a functional of the electron density. Phys Rev B 37:785–789. doi:10.1103/PhysRevB.37.785
34. Frisch MJ, Trucks GW, Schlegel HB, Scuseria GE, Robb MA, Cheeseman JR, Montgomery JA, Vreven T, Kudin KN, Burant JC, Millam JM, Iyengar SS, Tomasi J, Barone V, Mennucci B, Cossi M, Scalmani G, Rega N, Petersson GA, Nakatsuji H, Hada M, Ehara M, Toyota K, Fukuda R, Hasegawa J, Ishida M, Nakajima T, Honda Y, Kitao O, Nakai H, Klene M, Li X, Knox JE, Hratchian HP, Cross JB, Adamo C, Jaramillo J, Gomperts R, Stratmann RE, Yazyev O, Austin AJ, Cammi R, Pomelli C, Ochterski JW, Ayala PY, Morokuma K, Voth GA, Salvador P, Dannenberg JJ, Zakrzewski G, Dapprich S, Daniels AD, Strain MC, Farkas O, Malick DK, Rabuck AD, Raghavachari K, Foresman JB, Ortiz JV, Cui Q, Baboul AG, Clifford S, Cioslowski J, Stefanov BB, Liu G, Liashenko A, Piskorz P, Komaromi I, Martin RL, Fox DJ, Keith T, Al-Laham MA, Peng CY, Nanayakkara A, Challacombe M, Gill PMW, Johnson B, Chen W, Wong MW, Gonzalez C, Pople JA (2004) Gaussian 03, Revision D.01. Gaussian, Wallingford
35. Gonzalez C, Schlegel HB (1989) An improved algorithm for reaction path following. J Chem Phys 90:2154–2161. doi:10.1063/1.456010
36. Gonzalez C, Schlegel HB (1990) Reaction path following in mass-weighted internal coordinates. J Phys Chem 94:5523–5527. doi:10.1021/j100377a021
37. Blieger-König F, Schönbohn J (2002) AIM 2000 program package. Version 2.0. Büro für Innovative Software. Streibel Biegler-König, Bielefeld
38. Silva Lopez C, Faza ON, Cossío FP, York DM, de Lera AR (2005) Ellipticity: a convenient tool to characterize electrocyclic reactions. Chem Eur J 11:1734–1738. doi:10.1002/chem.200401026
39. Espinosa E, Alkorta I, Elguero J, Molins E (2002) From weak to strong interactions: a comprehensive analysis of the topological and energetic properties of the electron density distribution involving X–H···F–Y systems. J Chem Phys 117:5529–5542. doi:10.1063/1.1501133